Ca^{2+} leak through ryanodine receptor 1 regulates thermogenesis in resting skeletal muscle

Aldo Meizoso-Huesca[a], Luke Pearce[a], Christopher J. Barclay[a], and Bradley S. Launikonis[a,1]

[a]School of Biomedical Sciences, The University of Queensland, Brisbane, QLD 4072, Australia

Edited by Kurt Beam, Department of Physiology and Biophysics, Anschutz Medical Campus, University of Colorado Denver, Aurora, CO; received October 26, 2021; accepted December 13, 2021

Mammals rely on nonshivering thermogenesis (NST) from skeletal muscle so that cold temperatures can be tolerated. NST results from activity of the sarcoplasmic reticulum (SR) Ca^{2+} pump in skeletal muscle, but the mechanisms that regulate this activity are unknown. Here, we develop a single-fiber assay to investigate the role of Ca^{2+} leak through ryanodine receptor 1 (RyR1) to generate heat at the SR Ca^{2+} pump in resting muscle. By inhibiting a subpopulation of RyR1s in a single-fiber preparation via targeted delivery of ryanodine through transverse tubules, we achieve in-preparation isolation of RyR1 Ca^{2+} leak. This maneuver provided a critical increase in signal-to-noise of the SR-temperature-sensitive dye ER thermoyellow fluorescence signal from the fiber to allow detection of SR temperature changes as either RyR1 or SR Ca^{2+} pump activity was altered. We found that RyR1 Ca^{2+} leak raises cytosolic $[Ca^{2+}]$ in the local vicinity of the SR Ca^{2+} pump to amplify thermogenesis. Furthermore, gene-dose-dependent increases in RyR1 leak in *RYR1* mutant mice result in progressive rises in leak-dependent heat, consistent with raised local $[Ca^{2+}]$ at the SR Ca^{2+} pump via RyR1 Ca^{2+} leak. We also show that basal RyR Ca^{2+} leak and the heat generated by the SR Ca^{2+} pump in the absence of RyR Ca^{2+} leak is greater in fibers from mice than from toads. The distinct function of RyRs and SR Ca^{2+} pump in endothermic mammals compared to ectothermic amphibians provides insights into the mechanisms by which mammalian skeletal muscle achieves thermogenesis at rest.

skeletal muscle | thermogenesis | ryanodine receptor | SR Ca2+ pump | heat

Skeletal muscle plays a critical role in heat generation to establish the internal temperature of endothermals (1, 2). Pivotal to this, the sarcoplasmic reticulum (SR) Ca^{2+} pump constitutes 90% of the protein content of the SR membrane and is responsible for 30 to 50% of the basal metabolic rate of skeletal muscle (3, 4). SR Ca^{2+} pump thermogenic activity is modulated upon different conditions, including cold exposure, leading to an increase in basal energy expenditure and heat production through uncoupling of the pump. The SR membrane protein sarcolipin (5–8) and the SR membrane lipidic composition (9–11) have been proposed to be involved in this process. The alteration of the SR Ca^{2+} pump efficiency and subsequent increase in energy expenditure has been proposed as a mechanism to counter obesity (9–11).

The ryanodine receptor 1 (RyR1) has a major role in excitation–contraction coupling, releasing SR Ca^{2+} rapidly into the cytosol to regulate muscle contraction. However, in resting phases, the RyR1 passively leaks SR Ca^{2+} into the cytosol (12, 13). Despite this leakage, the SR Ca^{2+} content remains constant in resting muscle, indicating that the equivalent amount of leaked Ca^{2+} is resequestered into the SR via the SR Ca^{2+} pump. This SR Ca^{2+} leak–pump balance comes at the expense of adenosine triphosphate (ATP), causing heat to be generated as a by-product of ATP-dependent Ca^{2+} transportation into the SR.

Supporting a role of RyR1 Ca^{2+} leak in nonshivering thermogenesis (NST), cold exposure induces the phosphorylation of the RyR1 in mammals, destabilizing the channel and increasing the basal metabolic rate necessary to maintain the SR Ca^{2+} leak–pump balance (6, 14). A similar mechanism has been proposed in fish heater organs, where Ca^{2+} cycling between the SR and the cytosol sets a rate of the SR Ca^{2+} pump-dependent heat production that accounts for cranial endothermy (15–17).

Even though constitutive Ca^{2+} leak through the RyR1 has been observed in healthy human and rodent skeletal muscle (12, 13), no study has tested whether the leaked Ca^{2+} is directly involved in a regulated generation of heat by the SR Ca^{2+} pump. The small Ca^{2+} fluxes and associated heat changes in resting skeletal muscle have provided a major obstacle in studying the role of RyR1 Ca^{2+} leak in NST. Here, we present a single-fiber preparation, where RyR1 leak was locally inhibited within a defined section of the fiber, enabling us to determine the influence of RyR1 Ca^{2+} leak on the SR Ca^{2+} pump-dependent thermogenesis and the capacity of the SR Ca^{2+} pump to generate heat in the absence of RyR1 Ca^{2+} leak in mouse skeletal muscle at rest. Using this approach, we show that the heat generated by the SR Ca^{2+} pump in resting muscle is dependent on the magnitude of RyR1 Ca^{2+} leak through the establishment of a local $[Ca^{2+}]_{cyto}$ at the SR Ca^{2+} pump that is higher than the bulk $[Ca^{2+}]_{cyto}$. Additionally, we found the RyR1-independent thermogenic activity of the SR Ca^{2+} pump in situ to be the same across gain-of-function *RYR1* mutant mice that show a gene-dose-dependent increase in RyR1 Ca^{2+} leak, indicating that leak was defining muscle basal heat generation across the genotypes. In contrast, the heat generated due to basal SR Ca^{2+} pump activity and RyR Ca^{2+} leak in the muscle fibers of the ectothermic Queensland cane toad (*Rhinella marina*) was considerably lower than that

Significance

The evolution of mammals to use skeletal muscle as a source of heat allowed them to spread to all parts of the globe. The generation of heat requires increased adenosine triphosphate (ATP) hydrolysis in the resting muscle in a regulated manner, but how this mechanism works is unknown. The results suggest that mammals increase their RyR1 Ca^{2+} leak rate to amplify a basal ATP turnover rate at the sarcoplasmic reticulum Ca^{2+} pump that is higher than that of lower vertebrates. Muscle-based thermogenesis allows regulation of body temperature that is essential for life in mammals and provides a potential pathway for manipulating body weight or temperature by altering metabolic rate.

Author contributions: A.M.-H. and B.S.L. designed research; A.M.-H. and L.P. performed research; A.M.-H., L.P., C.J.B., and B.S.L. analyzed data; and A.M.-H. and B.S.L. wrote the paper.

The authors declare no competing interest.

This article is a PNAS Direct Submission.

[1]To whom correspondence may be addressed. Email: b.launikonis@uq.edu.au.

This article contains supporting information online at http://www.pnas.org/lookup/suppl/doi:10.1073/pnas.2119203119/-/DCSupplemental.

Published January 19, 2022.

observed in mouse, indicating that the properties of RyR and SR Ca^{2+} pump in the mammalian skeletal muscle are critical for this tissue to become a heat generator.

Results

In this section, we demonstrate the local inhibition of RyR1s by ryanodine applied through a targeted delivery via the transverse tubular-system (t-system) lumen and the use of this preparation to determine the effect of different magnitudes of RyR1 Ca^{2+} leak or known $[Ca^{2+}]_{cyto}$ on changes in the SR temperature. Our approach provides a reference condition, where RyR1 Ca^{2+} leak is locally blocked for the condition with functional RyR1s. This provides the signal-to-noise improvement required to resolve RyR1 Ca^{2+} leak-dependent heat generation within a single muscle fiber.

RyR1 Ca^{2+} Leak Increases SR Temperature. Single Tibialis Anterior (TA) muscle fibers from 12- to 16-wk-old mice were used in this study. Approximately 90% of the TA section used was glycolytic type IIB and X fibers (18–20). We isolated intact fibers under paraffin oil, and the sarcolemma of ∼60% of the fiber length was mechanically removed (Fig. 1*A*, step 1). The remaining intact fiber segment was exposed to an extracellular solution containing 50 μM ryanodine and 1 mM Fluo-5N using a 2-μL microcapillary tube (Fig. 1*A*, step 2). A concentration of 50 μM ryanodine irreversibly locks the RyR1 in a closed state (21, 22) and so was preferred to the use of other RyR inhibitors such as tetracaine (13), which displays reversibility upon solution exchanging. The paraffin oil surrounding the fiber restricts diffusion of extracellular solution delivered from the microcapillary tube to a localized region of the fiber, where the applied solution enters the t-system lumen. After ∼15 s, the external solution was removed, and the remaining sarcolemma of the fiber was peeled away (Fig. 1*A*, step 3). A well-known feature of the mechanical skinning procedure is that the t-system membrane seals over at its former interface with the surface of the fiber, trapping the extracellular solution inside the t-system (23, 24); consequently, the localized region of the fiber exposed to the extracellular solution containing the inhibitor can be visualized by tracking the Fluo-5N signal across the length of the fiber (Fig. 1 *A*–*C*).

To test whether ryanodine-exposed RyR1s were blocked, we exposed the fibers to 3 mM caffeine to induce cytosolic Ca^{2+} waves, a signature of RyR1 activity (Fig. 1*B*) (25–28). When added to the bathing solution, caffeine induced the appearance and propagation of Ca^{2+} waves. These waves occurred only across the section of the fiber without traces of Fluo-5N (Fig. 1 *C*–*E* and Movie S1). In contrast, Ca^{2+} waves propagated through fibers exposed to an external solution containing Fluo-5N and vehicle, indicating that the inhibition observed in Fig. 1C and Movie S1 is due to the presence of ryanodine. This result shows that the RyR1s of a restricted segment of a muscle fiber can be inhibited, allowing us to assess the contribution of the RyR1 in basal SR Ca^{2+} pump-dependent thermogenesis with an in-preparation reference section.

To measure the SR Ca^{2+} pump-mediated thermogenesis in resting muscle fibers, we loaded single fibers partially exposed to ryanodine and Fluo-5N (as described in Fig. 1*A*) with the temperature-sensitive dye ER thermo yellow (ERTY) that localizes specifically to the SR (*SI Appendix*, Fig. 1 *A* and *B*). ERTY fluorescence is inversely proportional to the SR temperature (29, 30). In contrast to the localized presence of Fluo-5N signal,

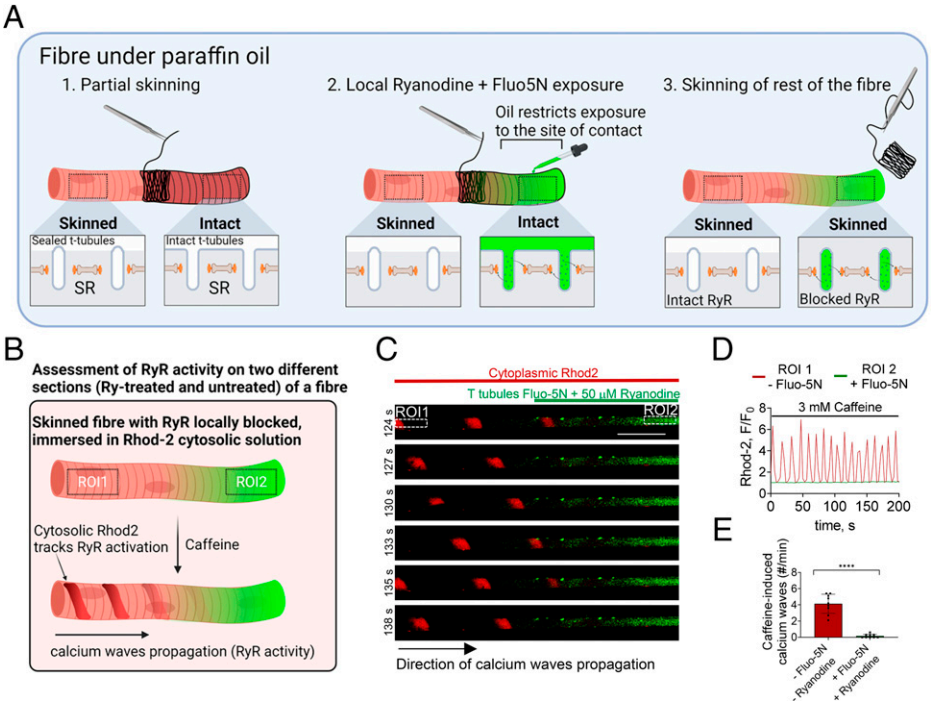

Fig. 1. Local inhibition of RyR1 within a restricted section of a skeletal muscle fiber. (*A*) Schematic diagram showing the local application of Fluo-5N and ryanodine in a single muscle fiber: step 1, mechanical skinning of ∼60% of the fiber. Step 2, exposure of the intact fiber segment to solution containing Fluo-5N and ryanodine with a microcapillary tube. Step 3, skinning of the remaining intact segment of the fiber. This three-step procedure performed under paraffin oil prevents the longitudinal diffusion of the Fluo-5N + ryanodine solution along the fiber. (*B*) Schematic representation of the assessment of RyR activity in a fiber locally exposed to ryanodine (Ry). (*C*) Representative xyt images of a single fiber locally exposed to extracellular Fluo-5N + ryanodine, bathed in a solution with rhod-2 and 3 mM caffeine to induce Ca^{2+} waves. (Scale bar: 150 μm.) (*D*) Spatially averaged rhod-2 signal over time from two independent regions of interest (ROI) indicated in *C*. ROI1, − Fluo-5N; ROI2, + Fluo-5N. (*E*) Summary of calcium waves per minute taking place in ROI1 (without Fluo-5N + ryanodine treatment) and ROI2 (with Fluo-5N + ryanodine treatment). Results are mean ± SD. Paired *t* test revealed statistical significance. ****$P < 0.0001$.

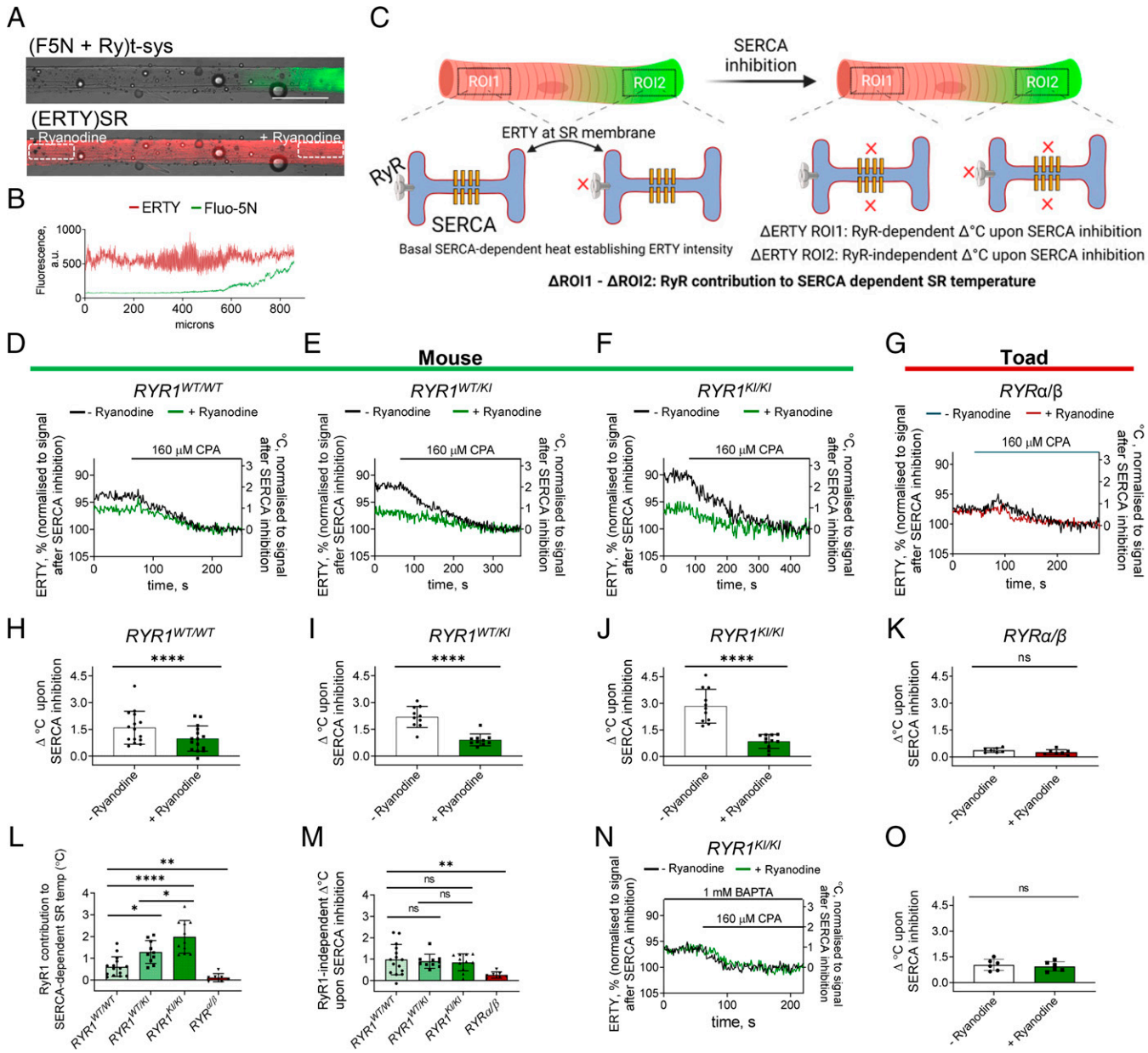

Fig. 2. RyR1 Ca2+ leak in resting muscle fibers contributes to the SR Ca^{2+} pump-mediated heat generation (*A*) Representative confocal image of a fiber partially exposed to Fluo-5N + ryanodine and loaded with 500 nM ERTY. (*B*) ERTY and Fluo-5N fluorescence profile across the long axis of the fiber shown in *A*. a.u., arbitrary units. (*C*) Schematic representation of the experiment to define RyR1 contribution to SR Ca^{2+} pump-dependent heat generation. (*D–G*) Representative traces showing the effect of 160 μM CPA on ERTY normalized fluorescence and Δ°C from two independent regions of interest (ROIs) of a single fiber without (black trace) and with ryanodine (colored trace) in *RYR1* KI mouse fibers $RYR1^{WT/WT}$ (*D*), $RYR1^{WT/KI}$ (*E*), and $RYR1^{KI/KI}$ (*F*); and toad *R. marina* *RYRα/β* fibers (*G*). (*H–K*) Summary of results of experiment shown in *D–G,* respectively. Paired *t* test. ns, not significant. $^{****}P < 0.001$. *n* values for *H–K*, respectively, are 15, 10, 11, and 7. (*L*) Summary of RyR contribution to the SR Ca^{2+} pump-dependent SR temperature. One-way ANOVA with Tukey's multiple comparisons revealed statistical significance across the mouse genotypes ($RYR1^{WT/WT}$ vs. $RYR1^{WT/KI}$, $P < 0.05$; $RYR1^{WT/WT}$ vs. $RYR^{KI/KI}$, $P < 0.0001$; $RYR1^{WT/KI}$ vs. $RYR1^{KI/KI}$, $P < 0.05$). *t* test with Welch's correction between $RYR1^{WT/WT}$ vs. *RYRα/β* ($P < 0.005$). (*M*) Summary of RyR-independent Δ °C upon SR Ca^{2+} pump inhibition. One-way ANOVA with Tukey's multiple comparisons revealed no statistical significance across *RYR1* KI fibers. *t* test with Welch's correction between $RYR1^{WT/WT}$ vs. *RYRα/β* ($P < 0.005$). (*N*) Representative traces showing the effect of CPA on ERTY normalized fluorescence and Δ °C on ROIs without (black trace) and with ryanodine (green trace) of a single $RYR1^{KI/KI}$ fiber. In this experiment, the fiber is bathed in 1 mM BAPTA. (*O*) Summary of experiment shown in *N*. Results are mean ± SD. Paired *t* test. ns, not significant. $n = 6$. SERCA, sarco(endo)plasmic reticulum Ca^{2+}-ATPase. $^{*}P < 0.05$, $^{**}P < 0.005$, $^{****}P < 0.0001$.

we observed a homogeneous ERTY signal across the long axis of the fiber (Fig. 2 *A* and *B*). Following the experimental protocol shown in Fig. 2*C*, we tested the contribution of a RyR1 Ca^{2+} leak on the SR Ca^{2+} pump-mediated heat generation in wild-type (WT; $RYR1^{WT/WT}$), heterozygous ($RYR1^{WT/KI}$), and homozygous ($RYR1^{KI/KI}$) mutant mouse muscle fibers carrying the *RYR1* gain-of-function variant p.G2435R to exploit the gene-dose-dependent increase in RyR1 Ca^{2+} leak across the three genotypes (31). In addition to these genotypes, fibers from the amphibian *R. marina* expressing *RYRα* and *RYRβ* genes instead of *RYR1* were tested to compare the role of RyR Ca^{2+} leak in SR Ca^{2+} pump-dependent thermogenesis between RyR1 and RyRα/β in the ectothermic toad. From these experiments, the RyR-dependent and -independent SR Ca^{2+} pump

heat generation were estimated by comparing ERTY normalized fluorescence before and after SR Ca^{2+} pump inhibition with cyclopiazonic acid (CPA) (ERTY fluorescence was normalized to the intensity after SR Ca^{2+} pump inhibition). The changes in ERTY fluorescence intensity (ΔERTY, %) were transformed to changes in degrees Celsius (Δ°C) by using the previously reported calibration (3.9%/°C) (29).

In the presence of RyR1 Ca^{2+} leak, the SR Ca^{2+} pump basal activity accounts for an increase in SR temperature of 1.6, 2.2, 2.8, and 0.4 °C in $RYR1^{WT/WT}$, $RYR1^{WT/KI}$, $RYR1^{KI/KI}$, and $RYR\alpha/\beta$ fibers, respectively (Fig. 2 *D–G*, black traces). Conversely, the basal SR temperature shift set by the SR Ca^{2+} pump ATP hydrolysis in the absence of RyR1 Ca^{2+} leak was 1, 0.9, 0.9, and 0.3 °C in $RYR1^{WT/WT}$, $RYR1^{WT/KI}$, $RYR1^{KI/KI}$, and $RYR\alpha/\beta$, respectively (Fig. 2 *D–G*, green traces). In each mammalian genotype, the SR Ca^{2+} pump-dependent SR temperature in the presence of RyR1 Ca^{2+} leak was higher than in the absence of RyR1 Ca^{2+} leak (Fig. 1 *H–J*), showing that RyR1 Ca^{2+} leak in resting muscle fibers contributes to the basal thermogenic activity of the SR Ca^{2+} pump in mammalian muscle (Movie S3). In contrast, the SR Ca^{2+} pump-dependent SR resting temperature was not affected by RyRα/β leak in amphibian muscle (Fig. 2*K*).

From the results shown in Fig. 2 *H–K*, we calculated the RyR1 contribution to the SR Ca^{2+} pump-dependent SR temperature by subtracting the RyR-independent from the RyR-dependent Δ°C upon SR Ca^{2+} pump-inhibition values from the same fiber (Fig. 2*C*). Within the mammalian groups, the RyR1 contribution to the SR Ca^{2+} pump-dependent SR temperature progressively increased from the most stable to the leakiest RyR1s ($RYR1^{WT/WT}$ < $RYR1^{WT/KI}$ < $RYR1^{KI/KI}$) (Fig. 2*L*). In addition, RyR Ca^{2+} leak contribution in $RYR\alpha/\beta$ was lower than in $RYR1^{WT/WT}$, suggesting that RyR1 Ca^{2+} leak provides a thermogenic source that skeletal muscle fibers with RyRα/β lack.

When the RyR1 Ca^{2+} leak was blocked (RyR1-independent Δ°C upon the SR Ca^{2+} pump inhibition), the three mammalian genotypes showed the same Δ°C change upon inhibition of the pump (Fig. 2*M*). In contrast, RyR-independent Δ°C change upon the SR Ca^{2+} pump inhibition was lower in $RYR\alpha/\beta$ (0.3 °C) compared to $RYR1^{WT/WT}$ (1 °C). Collectively, these results show that 1) in resting WT fibers, the SR Ca^{2+} pump basal activity shifts the SR temperature 1.6 °C, where 0.6 °C of that shift comes from the constitutive RyR1 Ca^{2+} leak; 2) increases in RyR1 Ca^{2+} leak lead to an increase in heat generation by the SR Ca^{2+} pump in resting skeletal muscle; and 3) in fibers with RyR α and β subtypes instead of RyR1, RyR Ca^{2+} leak is not a significant source of heat generation in resting skeletal muscle.

Next, we checked whether the increase in the SR Ca^{2+} pump heat generation exerted by RyR1 Ca^{2+} leak relied on cytosolic Ca^{2+} diffusion from the channel to the pump. To do this, we restricted the cytosolic Ca^{2+} diffusion by substituting the cytosolic Ca^{2+} buffer 0.1 mM ethylene glycol-*bis*(β-aminoethyl ether)-*N*,*N*,*N*′,*N*′-tetraacetic acid (EGTA) for 1 mM 1,2-*bis*(o-aminophenoxy)ethane-*N*,*N*,*N*′,*N*′-tetraacetic acid (BAPTA). In contrast to EGTA, BAPTA (1 mM) is a fast Ca^{2+} buffer that restricts the distance that a Ca^{2+} ion can travel freely before being chelated to 22.4 nm (13). To maximize the sensitivity of our assay, we tested the effect of CPA in the SR temperature of $RYR1^{KI/KI}$ fibers in the presence of BAPTA. These fibers were used in contrast to $RYR1^{WT/WT}$ or $RYR^{WT/KI}$ fibers because of their higher contribution of RyR1 Ca^{2+} leak to thermogenesis (Fig. 2*J*). Therefore, the $RYR1^{KI/KI}$ fibers should be the most sensitive to a restriction in cytoplasmic Ca^{2+} diffusion. Before testing the effect of cytoplasmic BAPTA on RyR1-dependent SR Ca^{2+} pump heat generation, we confirmed that the SR Ca^{2+} loading was comparable under the same $[Ca^{2+}]_{cyto}$ (100 nM) in EGTA or BAPTA (*SI Appendix*, Fig. 2). When CPA was applied to $RYR1^{KI/KI}$ fibers partially exposed to ryanodine, the ERTY transients in sections with and without functional RyR1s were not different (P = 0.576; 4.053 ± 0.529% and 3.693 ± 0.442%, respectively) and were comparable to the values observed in ryanodine-exposed $RYR1^{KI/KI}$ fibers in 0.1 mM EGTA (Fig. 2 *N* and *O*). This shows that cytosolic Ca^{2+} diffusion from the RyR1 to the SR Ca^{2+} pump is required to increase the SR Ca^{2+} pump activity and heat generation.

Low $[Ca^{2+}]_{cyto}$ Levels Regulate Heat Generation in Healthy, Resting Muscle. An increase in RyR1 Ca^{2+} leak has been proposed as a mechanism to maintain body temperature upon chronic cold exposure, where the increase in leak leads to greater SR Ca^{2+} pump activity to maintain the SR Ca^{2+} leak/uptake balance (6). Therefore, it is expected that mild changes in $[Ca^{2+}]_{cyto}$ alter the activity of the pump in healthy muscle. To test this hypothesis, we coloaded WT muscle fibers with ERTY and fluo-5N in the SR to track changes in SR temperature and $[Ca^{2+}]_{SR}$, respectively, during exposure to increasing $[Ca^{2+}]_{cyto}$ below the $[Ca^{2+}]_{cyto}$ threshold for contraction (32) (Fig. 3). Increasing $[Ca^{2+}]_{cyto}$ from 67 nM to 136 nM increased the $[Ca^{2+}]_{SR}$, but no change in ERTY was observed. However, an increase to 165 nM $[Ca^{2+}]_{cyto}$ caused a significant change in both $[Ca^{2+}]_{SR}$ (165 vs. 67 and 165 vs. 91 nM) and ERTY (165 vs. 67 and 165 vs. 91 nM), indicating an increase in heat generation. These results show that small changes in $[Ca^{2+}]_{cyto}$ can produce a significant increase in SR Ca^{2+} pump thermogenic activity in WT muscle fibers.

RyR1 Ca^{2+} Leak Increases Local $[Ca^{2+}]_{cyto}$ at SR Ca^{2+} Pump for Heat Generation. The rise in the SR Ca^{2+} pump-dependent thermogenesis generated by increases in RyR1 Ca^{2+} leak in mouse fibers (Fig. 2 *D–F*) and the reliance of the SR Ca^{2+} pump thermogenic activity on Ca^{2+} diffusion from the channel to the pump (Fig. 2 *N* and *O*) suggest that RyR1 Ca^{2+} leak sets a local $[Ca^{2+}]_{cyto}$ at the SR Ca^{2+} pump higher than the bulk $[Ca^{2+}]_{cyto}$, set in our experiments to 100 nM. To calculate the local $[Ca^{2+}]_{cyto}$ at the SR Ca^{2+} pump set by RyR1 Ca^{2+} leak, we generated a calibration curve of ERTY signal across a range of $[Ca^{2+}]_{cyto}$ (500 to 50 nM) at the SR Ca^{2+} pump. For this calibration, RyR1 was blocked with 1 mM Tetracaine so that RyR1 Ca^{2+} leak did not influence $[Ca^{2+}]_{cyto}$. Fibers were initially bathed in 500 nM Ca^{2+} solution and progressively subjected to decreasing $[Ca^{2+}]_{cyto}$ solutions (Fig. 4*A*). The average ERTY value from the last 30 s of each condition was calculated (Fig. 4*B*) and used to plot a curve of $[Ca^{2+}]_{cyto}$ vs. ERTY (%) (Fig. 4*C*). Notably, the greatest changes in ERTY signal were achieved between 300 and 100 nM $[Ca^{2+}]_{cyto}$. Particularly, from 200 to 150 nM ERTY, fluorescence intensity increased from 104.984 ± 0.252 to 108.298 ± 0.313%, whereas from 150 to 100 nM, the intensity increased from 108.298 ± 0.319 to 113.163 ± 1.021%. To verify this result, an experiment was performed where the fiber was subjected to increasing concentrations of Ca^{2+} from 50 to 500 nM. A similar relationship between ERTY signal and $[Ca^{2+}]_{cyto}$ was observed (*SI Appendix*, Fig. 3).

To calculate the contribution of RyR1 Ca^{2+} leak on the local $[Ca^{2+}]_{cyto}$ at the SR Ca^{2+} pump, we used the previously obtained values of RyR1 contribution to ΔERTY (%) upon SR Ca^{2+} pump inhibition (Fig. 4*D*) in conjunction with the generated $[Ca^{2+}]_{cyto}$ vs. ERTY (%) curve. Since the RyR1 leak contribution to ΔERTY (%) values were obtained from experiments performed at 100 nM $[Ca^{2+}]_{cyto}$, the ERTY % of fluorescence value at 100 nM Ca^{2+} within the calibration curve (113.162 ± 1.021%) was used as a reference value (Fig. 4*E*). We subtracted the values of RyR1 contribution to ΔERTY corresponding to 2.393 ± 0.456%, 5.025 ± 0.648%, and 7.747 ± 0.884% for $RYR1^{WT/WT}$, $RYR1^{WT/KI}$, and $RYR1^{KI/KI}$, respectively, to the percentage of fluorescence at 100 nM Ca^{2+} in the calibration curve. The obtained values were interpolated in the curve shown in Fig. 4*C* to estimate their corresponding values of $[Ca^{2+}]_{cyto}$. Using this calculation, with the bulk $[Ca^{2+}]_{cyto}$ set to 100 nM, RyR1

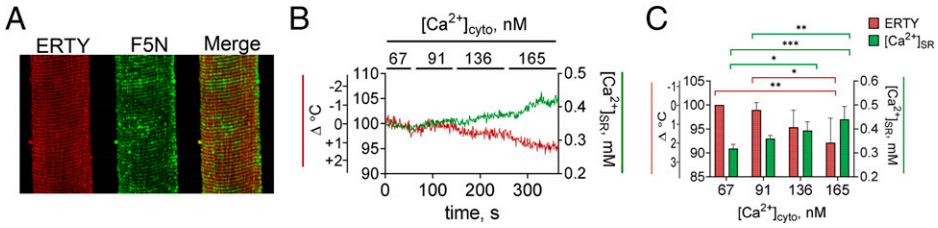

Fig. 3. Mild increases in $[Ca^{2+}]_{cyto}$ up-regulate the thermogenic activity of the SR Ca^{2+} pump. (*A*) Representative confocal image of a fiber coloaded with 500 nM ERTY and 10 μM Fluo-5N inside the SR. (*B*) $_{free}[Ca^{2+}]_{SR}$ (green) and normalized ERTY fluorescence (red) over time from a muscle fiber sequentially exposed to increasing concentrations of cytoplasmic calcium ($[Ca^{2+}]_{cyto}$). (*C*) Summary of $_{free}[Ca^{2+}]_{SR}$ values collected from the exposure to increasing $[Ca^{2+}]_{cyto}$. One-way ANOVA with Tukey's multiple comparisons revealed statistical significances (67 vs. 136, $P = 0.0156$; 67 vs. 165, $P = 0.0002$; 91 vs. 165, $P = 0.0095$). Summary of ERTY signal (%, normalized to baseline at 67 nM $[Ca^{2+}]_{cyto}$). Results are mean ± SD. One-way ANOVA with Tukey's multiple comparisons revealed statistical significances (67 vs. 165, $P = 0.0065$; 91 vs. 165, $P = 0.0185$); $n = 5$. $^*P < 0.05$, $^{**}P < 0.01$, $^{***}P < 0.001$.

leakiness progressively increased the local $[Ca^{2+}]_{cyto}$ at the SR Ca^{2+} pump to 125 ± 6, 157 ± 8, and 195 ± 14 nM $[Ca^{2+}]_{cyto}$ in $RYR1^{WT/WT}$, $RYR1^{WT/KI}$, and $RYR1^{KI/KI}$, respectively (Fig. 4*F*). These results are consistent with RyR1 Ca^{2+} leak setting a local $[Ca^{2+}]_{cyto}$ at the SR Ca^{2+} pump that drives its activity.

Next, we used the estimates of local $[Ca^{2+}]_{cyto}$ at the SR Ca^{2+} pump in the three *RYR1* genotypes to determine the SR Ca^{2+} pump ATP consumption rates and heat output using our previously established model (33). Fig. 5*A* shows the relationship of the SR Ca^{2+} pump ATP consumption rate (in μM/s) across the range of $[Ca^{2+}]_{cyto}$ from 50 to 500 nM. The ATP consumption rate increased with increasing RyR1 leakiness across the genotypes (51.2 ± 5.3, 78.3 ± 8.5, and 126.8 ± 17.2 μM/s for $RYR1^{WT/WT}$, $RYR1^{WT/KI}$, and $RYR1^{KI/KI}$ fibers, respectively [Fig. 5*B*]).

In WT fibers, with the RyR1 blocked and the local $[Ca^{2+}]_{cyto}$ at the SR Ca^{2+} pump the same as the bulk $[Ca^{2+}]_{cyto}$ (100 nM), the estimated SR Ca^{2+} pump ATPase rate was 30.7 μM/s. In contrast, with RyR1 Ca^{2+} leak present and local $[Ca^{2+}]_{cyto}$ at the SR Ca^{2+} pump raised to 125 nM Ca^{2+}, the SR Ca^{2+} pump ATPase rate was 51.2 μM/s. This indicates that a 25% increase in $[Ca^{2+}]_{cyto}$ at the pump leads to a 66% increase in the SR Ca^{2+} pump activity (Fig. 5*C*). This nonlinear increase in the relationship between $[Ca^{2+}]_{cyto}$ and ATP consumption translates to an equivalent increase in the SR Ca^{2+} pump-dependent heat production in resting muscle. This suggests that the Ca^{2+} handling properties of the SR Ca^{2+} pump coupled with the endogenous cytosolic Ca^{2+} environment allow the pump to amplify the Ca^{2+} cycling-dependent heat production in response to RyR1 Ca^{2+} leak.

Finally, we used the estimated ATP consumption rate values to calculate the SR Ca^{2+} pump-dependent heat production at rest across the three genotypes. Assuming that in a steady state, ATP is regenerated through glucose oxidation (enthalpy change for this process is 2,802 kJ/mol at a stoichiometry of 38 ATP per glucose) at the same rate that it is consumed, the heat output is

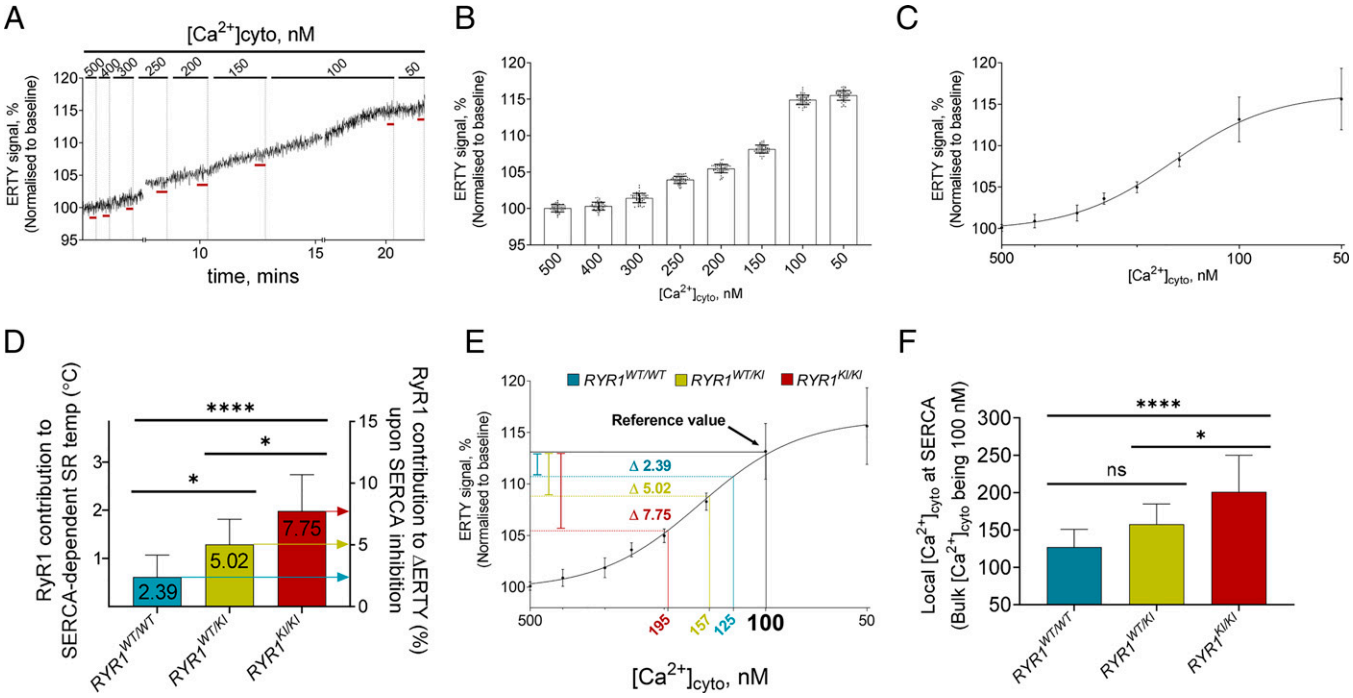

Fig. 4. RyR1 Ca^{2+} leak sets a local $[Ca^{2+}]_{cyto}$ at the SR Ca^{2+} pump higher than the bulk $[Ca^{2+}]_{cyto}$. (*A*) ERTY normalized fluorescence profile from a single mechanically skinned fiber exposed to decreasing concentrations of $[Ca^{2+}]_{cyto}$ from the range of 500 nM to 50 nM. (*B*) Summary of ERTY fluorescence intensity values during the last 30 s of each $[Ca^{2+}]_{cyto}$ condition from trace shown in *A*. (*C*) Four parameters calibration curve of $[Ca^{2+}]_{cyto}$ vs. ERTY signal (%). $R^2 = 0.91$. $n = 7$. (*D*) RyR1 contribution to ΔERTY upon SR Ca^{2+} Pump inhibition across the three genotypes ($RYR1^{WT/WT}$, $RYR1^{WT/KI}$, and $RYR1^{KI/KI}$). (*E*) Interpolation of mean values of RyR1-dependent ΔERTY(%) of the three genotypes on $[Ca^{2+}]_{cyto}$ vs. ERTY signal calibration curve. (*F*) Summary of local $[Ca^{2+}]_{cyto}$ at the SR Ca^{2+} pump across the three genotypes. Results are mean ± SD. One-way ANOVA with Tukey's multiple comparisons revealed statistical significance across the genotypes ($RYR1^{WT/WT}$ vs. $RYR1^{KI/KI}$, $P < 0.0001$; $RYR1^{WT/KI}$ vs. $RYR1^{KI/KI}$, $P = 0.0169$). $^*P < 0.05$, $^{****}P < 0.0001$, ns, not significant.

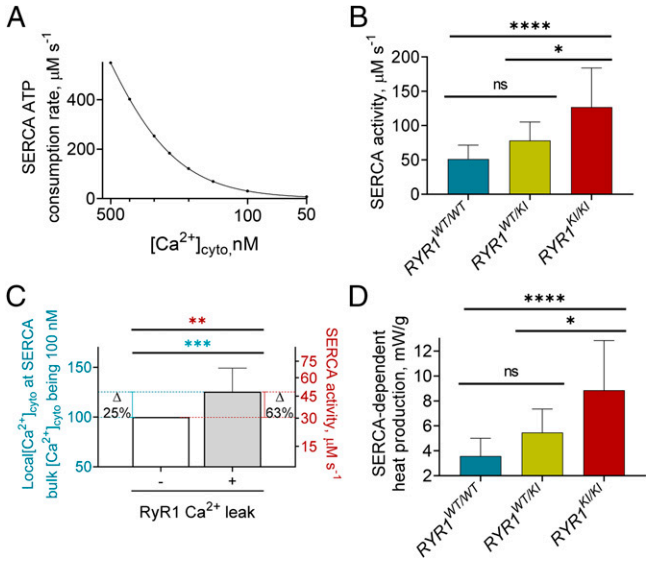

Fig. 5. Local $[Ca^{2+}]_{cyto}$ at the SR Ca^{2+} pump sets the SR Ca^{2+} pump thermogenic activity. (*A*) Model of the SR Ca^{2+} pump ATP consumption rate across a range of 500 to 50 nM $[Ca^{2+}]_{cyto}$. (*B*) The SR Ca^{2+} pump activity (in μM/s) given the estimated local $[Ca^{2+}]_{cyto}$ at the pump across the three genotypes. One-way ANOVA with Tukey's multiple comparisons revealed statistical significance across the genotypes ($RYR1^{WT/WT}$ vs. $RYR1^{KI/KI}$, $P < 0.0001$; $RYR1^{WT/KI}$ vs. $RYR1^{KI/KI}$, $P = 0.0135$). (*C*) Summary of local $[Ca^{2+}]_{cyto}$ at the SR Ca^{2+} pump in $RYR1^{WT/WT}$ in absence and presence of RyR1 Ca^{2+} leak (left *y* axis) ($P < 0.001$) compared to the SR Ca^{2+} pump activity at the given local $[Ca^{2+}]_{cyto}$ concentrations at the SR Ca^{2+} pump in both conditions (right *y* axis) ($P < 0.01$). (*D*) The SR Ca^{2+} pump-dependent heat production (in mW/g) across the three genotypes given the estimated the SR Ca^{2+} pump activity values shown in *B*. Results are mean ± SD. One-way ANOVA with Tukey's multiple comparisons revealed statistical significance across the genotypes ($RYR1^{WT/WT}$ vs. $RYR1^{KI/KI}$, $P < 0.0001$; $RYR1^{WT/KI}$ vs. $RYR1^{KI/KI}$, $P = 0.0135$). *$P < 0.05$, **$P < 0.01$, ***$P < 0.001$, ****$P < 0.0001$, ns, not significant.

2,802 kJ/38 mol = 74 kJ/mol (corresponding to heat produced per ATP generated). At the calculated SR Ca^{2+} pump, ATP consumption rates estimated for $RYR1^{WT/WT}$, $RYR1^{WT/KI}$, and $RYR1^{KI/KI}$, the heat output is ATP consumption × heat produced per ATP/muscle density: 51.2 μM/s × 74 kJ/mol/1,060 g/L = 3.57 mW/g, 78.3 μM/s × 74 kJ/mol/1,060 g/L = 5.46 mW/g, and 126.8 μM/s × 74 kJ/mol/1,060 g/L = 8.85 mW/g for $RYR1^{WT/WT}$, $RYR1^{WT/KI}$, and $RYR1^{KI/KI}$, respectively (Fig. 5*D*).

This data quantitatively describe the role of RyR1 in the SR Ca^{2+} pump-mediated heat generation in resting mammalian skeletal muscle by constitutively feeding the activity of the pump and that modulation of this input produces a nonlinear alteration in the SR Ca^{2+} pump ATP consumption and heat production.

Discussion

The evidence presented here shows that SR Ca^{2+} leak through the RyR1 directly affects the local $[Ca^{2+}]_{cyto}$ at the SR Ca^{2+} pump in mammalian resting skeletal muscle fibers, setting the thermogenic activity of the pump. We show that the SR Ca^{2+} pump contribution to SR temperature in resting skeletal muscle is different in mouse and toad skeletal muscle, examples of endotherms and ectotherms, respectively. The differences between the mouse and toad fibers at the SR was the heat generated by the isolated SR Ca^{2+} pump in the fiber and the additional contribution of Ca^{2+} via RyR leak to further amplify heat generation at the pump. In the *RYR1* KI mouse, it was not possible to resolve a difference in heat generated across the genotypes of the isolated SR Ca^{2+} pump in the fiber. This result indicates that RyR Ca^{2+} leak provides amplification of the heat generated by the pump by proportionally raising the local $[Ca^{2+}]$ at the pump in the resting fiber. Additionally, the lack of sarcolipin in the SR of TA fibers does not prevent the SR Ca^{2+} from generating significant heat, certainly in comparison to the toad, and the consistent heat generated by the isolated SR Ca^{2+} pump in the *RYR1* KI fibers suggests that the composition of the SR is comparable between the genotypes.

To make measurements of the heat generated by the SR in resting muscle, we used a single-fiber approach, employing a targeted local inhibition of RyR1s with ryanodine delivered through the t-system. Ryanodine was chosen as the RyR inhibitor because of its high affinity for the target, which maintained binding to the RyR after the preparation was transferred from oil to a cytoplasmic bathing solution that did not contain ryanodine. The presence of a reference section in a single fiber where RyR1s were inhibited increased the signal-to-noise for detecting changes in RyR1 Ca^{2+} leak-dependent changes in SR temperature. Loading of the temperature-sensitive dye was not affected by local inhibition of RyR1s, and the presence of both conditions (± RyR1 Ca^{2+} leak) within the same biological sample allowed us to assess its contribution under the same dye-loading and acquisition settings.

RyR1 Ca^{2+} leak sets a standing Ca^{2+} gradient between the RyR1s and the SR Ca^{2+} pump, where the local $[Ca^{2+}]_{cyto}$ at the SR Ca^{2+} pump was maintained at a value greater than the bulk $[Ca^{2+}]_{cyto}$. This feature allows the Ca^{2+}-handling properties of the SR to set the basal use of ATP at the SR Ca^{2+} pump, setting the heat output. We were able to show that the magnitude of RyR1 Ca^{2+} leak is critical to heat generation by the SR by examining the SR Ca^{2+} pump-dependent heat generation of *RYR1* KI mouse muscle fibers that show a gene-dose-dependent increase in RyR1 Ca^{2+} leak (31). In contrast, the ectothermic toad showed a smaller change in SR temperature. This is partially explained by the lower capacity of the toad fibers to leak Ca^{2+} through the RyR compared to mouse, where evidence suggests that Ca^{2+} leakage through RyRs in toad fibers is one order of magnitude lower than in mammals (34, 35).

We provide direct evidence that local $[Ca^{2+}]$ at the SR Ca^{2+} pump increases the pump basal activity and heat generation in healthy, resting mammalian skeletal muscle. Across a range of $[Ca^{2+}]_{cyto}$ in the resting muscle, the SR Ca^{2+} pump generated a nonlinear increase in SR temperature. This result indicates that thermogenic gain of the muscle is sensitive to small changes in RyR1 Ca^{2+} leak when the basal heat-generating capacity of the pump was relatively high, as in mouse muscle. The generation of a standing Ca^{2+} gradient set by the SR is consistent with raised $[Ca^{2+}]$ in the junctional space between the t-system and SR terminal cisternae, compared to the bulk cytoplasm, as shown previously by monitoring $[Ca^{2+}]_{t\text{-}sys}$ levels in the presence and absence of RyR1 Ca^{2+} leak (13).

In the absence of RyR1 Ca^{2+} leak, the SR Ca^{2+} pump continued to generate heat in the fiber. The constant generation of heat indicates a basal ATP hydrolysis rate. Ca^{2+} slippage from the SR lumen to the cytoplasm through the pump, under a local build-up of adenosine diphosphate (36, 37), will generate a loss of SR Ca^{2+} that would require constant resequestering of Ca^{2+} to maintain the SR Ca^{2+} content. Importantly, the heat generated by the isolated SR Ca^{2+} pump provides a critical basal level that can be further amplified by RyR1 Ca^{2+} leak. The stark difference in heat generated by the isolated SR Ca^{2+} pump in mouse and toad fibers thus underscores the capacity of the resting muscle in these animals to act as a heat generator. The greater level of heat generated by the SR pump of the mouse than the toad isolated pump is likely set by differences in the SR Ca^{2+} pump modulation through regulatory proteins that interact with the pump and the lipidic composition where the SR Ca^{2+} pump is embedded, altering ATP hydrolysis–Ca^{2+} transport coupling ratios (5, 38). Furthermore, the fast-twitch fibers from

TA used in this study do not contain sarcolipin (39), indicating that sarcolipin is not critical to the reduction in coupling efficiency of the SR Ca^{2+} pump. Across the muscle fibers in the body, the SR Ca^{2+} pump could be further regulated by sarcolipin, reactive oxygen species, phospholamban, heat shock proteins, and other regulators (5, 40), which vary in expression across fiber types (39) and possibly other factors.

From our calibration of the $[Ca^{2+}]_{cyto}$ at the SR Ca^{2+} pump and the heat generated, we were able to show how leakier RyRs in fibers from the *RYR1* KI mice provide more Ca^{2+} to the pump under the same bulk $[Ca^{2+}]_{cyto}$ (Figs. 4 and 5). In the toad fibers, the low contribution of Ca^{2+} leak to heat generation at the pump may be, in part, due to a relatively low $[Ca^{2+}]_{SR}$ restricting the driving force for leak (41, 42). Additionally, the two sets of junctional membranes per sarcomere in mammalian fibers compared to one in amphibians (43) may increase the density of RyRs and SR Ca^{2+} pumps and decrease the diffusional distance for Ca^{2+} to travel in mice to increase the $[Ca^{2+}]$ at the SR Ca^{2+} pump compared to toads.

Our direct demonstration that skeletal muscle fibers can change their level of heat generation by changing RyR1 Ca^{2+} leak and setting a high basal level of heat generation solely through the SR Ca^{2+} pump provides key insights into how mammals can stay warm in a wide range of environments. Skeletal muscle is a large organ that is highly specialized for the handling of Ca^{2+}, providing a source of heat generation at every sarcomere. The ability of mammals to adapt the Ca^{2+} handling apparatus of skeletal muscle under resting conditions for the purpose of generating volumes of heat that maintain body temperature (5) was a critical evolutionary step that allowed mammals to colonize all parts of the globe. Importantly, this evolutionary step involved altering the SR so that the pump became less efficient, consuming more energy at rest than ectothermic vertebrates, and, equally, the RyR1 provides an amplifier of the heat that can be generated at the pump to assist meeting the thermogenic need of the mammal. Furthermore, the sensitive method developed here to detect heat in a resting fiber with an in-preparation control for the RyR leak can be applied to any skeletal muscle fiber from vertebrates. For example, the contribution of the RyR leak and the isolated SR Ca^{2+} pump to SR heat generation can be assessed across fiber types and in models of aging and sarcopenia, exercise, and numerous other lifestyle and genetic factors. The results may form a basis for understanding changes in whole-body metabolism.

Methods

Muscle Preparation. All experimental methods using animals were approved by the Animal Ethics Committee at The University of Queensland. Male C57BL/6J mice were euthanized by cervical dislocation, and the TA muscles were rapidly excised. Cane toads were stunned with a blow to the head and double pithed, and the iliofibularis muscles were dissected. Muscles were then placed in a Petri dish under paraffin oil above a layer of Sylgard.

All chemicals were obtained from Sigma-Aldrich. Ryanodine, Tetracaine, CPA, and *N*-benzyl-*p*-toluene sulfonamide (BTS) were prepared in stocks dissolved in dimethyl sulfoxide (DMSO).

Localized Inhibition of RyR1s within a Single Muscle Fiber. Single fibers from TA muscles were isolated by using fine forceps. To expose discrete segments of single fibers immersed on paraffin oil to Ryanodine, the fibers were mechanically skinned, leaving an approximate 500-μm subsection of the fiber with the sarcolemma intact. The intact section of the fiber was exposed to a solution containing 50 μM Ryanodine, (the following in mM) Fluo-5N, 1; $CaCl_2$, 2.5; NaCl, 132; $MgCl_2$, 1; KCl, 3.3; and Hepes, 20 (pH 7.4), using a 2-μL microcapillary tube. The localized application of ryanodine was possible due to 1) the restriction on diffusion set by the paraffin oil surrounding the intact fiber and physiological solution applied to it (44); and 2) the restriction on longitudinal diffusion of small molecules within the t-system (45). After the 10 s of exposure, the remaining intact section of fiber was mechanically skinned. The preparation was transferred to a custom-built chamber and placed under 50 μL of K^+-based cytoplasmic solution containing (in mM): Mg^{2+}, 1; $EGTA_{total}$, 0.1; Hepes, 90; K^+, 126; Na^+, 36; ATP, 8; creatine phosphate, 10; and BTS, 0.05, with pH adjusted (with KOH) to 7.1. Free $[Ca^{2+}]$ was set to 100 nM for imaging on the confocal microscope. The [EGTA] was set at 0.1 mM so that the SR Ca^{2+} pump outcompeted the EGTA for access to the Ca^{2+} leaked through the RyR. This allowed the endogenous SR Ca^{2+} content and leak to be preserved in experiments as the local $[Ca^{2+}]_{cyto}$ increased at the SR Ca^{2+} pump due to RyR Ca^{2+} leak (31).

Confocal Imaging. Mounted skinned fibers were imaged by using an Olympus FV1000 confocal microscope equipped with an Olympus 0.7-numerical aperture 20x Plan-Apochromat objective. Fluo-5N trapped in the sealed t-system was excited with 488-nm HeNe laser; cytoplasmic rhod-2 or ERTY were excited with 543-nm HeNe laser. Emission was filtered by using the Olympus spectra detector. To track caffeine-induced Ca^{2+} transients or CPA-induced ERTY transients, images were continuously recorded in xyt mode using an aspect ratio of 2,048 × 256 pixels, with the *x* axis of the image parallel long axis of the fiber to capture 890 μm of fiber length and analyze representative sections of the fiber with and without t-system Fluo-5N signal within the same experiment. Frame capture rate was 1.3 s.

Cytosolic Calcium Waves. Calcium waves were induced by exposing single fibers to 3 mM caffeine bathed in a cytosolic solution (described above) containing Rhod 2 (10 mM) with pH adjusted (with KOH) to 7.1.

ERTY and Fluo-5N SR Loading. Single muscle fibers were bathed in a cytoplasmic solution (same formulation as above) with 500 nM ERTY for 40 min at 37 °C. ERTY loading solution was prepared from 100 μM ERTY aliquots dissolved in DMSO.

Fluo-5N acetoxymethyl (AM) was used to monitor SR Ca^{2+} concentration. Single fibers were bathed in cytoplasmic solution (same formulation as above) with 10 μM Fluo-5N AM ester, and 10 μM carbonylcyanide *p*-trifluoromethoxyphenylhydrazone and 0.05% Pluronic F-127 detergent were added to decouple mitochondria and to help disperse the AM ester, respectively. Fibers were incubated for 40 mins at 37 °C.

For both dyes loading, after incubation time, the fibers were washed twice with cytoplasmic solution in the absence of dye.

Image analysis for SR Ca^{2+} measurements. SR Fluo-5N fluorescence ($F(t)$) was collected during continuous xyt imaging. At the end of the experiment, fibers were exposed to solution containing 50 μM ionomycin and 5 mM Ca^{2+}, followed by a solution with 0 Ca^{2+} to obtain the fluorescence maximum (Fmax) and minimum (Fmin), respectively. The previously determined K_D of Fluo-5N in the SR [0.4 mM (42)] was used to determine $[Ca^{2+}]_{SR}$, with the relationship:

$$[Ca^{2+}]_{SR}(t) = k_{D,Ca} * (F(t)–Fmin)/(Fmax–F(t)).$$

In the experiments where the Fmax solution induced vacuoles, Fluo-5N signal could not be used as a suitable calibration point for the determination of $[Ca^{2+}]_{SR}$. Under such conditions, Fmax was determined by rearranging the equation described above:

$$Fmax = F + (F - Fmin) * K_{D,Ca}/[Ca^{2+}]_{SR},$$

with F and $[Ca^{2+}]$, the respective free Ca^{2+} concentration in the cytoplasm (100 nM) and the SR (calibrated in an independent set of experiments), respectively.

ERTY vs. $[Ca^{2+}]$Cyto Calibration Curve. Fibers were initially bathed in 500 nM Ca^{2+} solution and progressively exposed to decreasing $[Ca^{2+}]_{cyto}$ solutions (500→400→300→250→200→150→100→50 nM Ca^{2+}). Each Ca^{2+} bathing solution was maintained for either a minute or for the necessary time for the ERTY fluorescence intensity to reach a 30-s plateau. These experiments were performed in constant presence of 1 mM Tetracaine to discard any contribution of RyR1 channels.

SR Ca^{2+} Pump ATP Consumption Modeling. The SR Ca^{2+} pump ATP consumption rates were modeled establishing a sigmoidal relationship between $[Ca^{2+}]_{cyto}$ and the rate of the SR Ca^{2+} pumping (46). For this model, we estimated the maximum rate of SR Ca^{2+} pumping from the rate of skeletal muscle heat production during an isometric contraction (47).

Statistical Analysis. Statistical analysis was performed with GraphPad Prism 8. Paired *t* test was used to compare the CPA-induced ERTY transients in the presence and absence of ryanodine treatment within the same preparation. A one-way ANOVA with Tukey's multiple comparisons was used to compare the RyR1-dependent and RyR1-independent ΔERTY upon SR Ca^{2+} pump inhibition across the different genotypes, as well as ERTY fluorescence intensity and $[Ca^{2+}]_{SR}$ across mild increases in $[Ca^{2+}]_{cyto}$ and local $[Ca^{2+}]_{cyto}$ at the SR

Ca^{2+} pump, the SR Ca^{2+} pump ATP consumption rate, and the SR Ca^{2+} pump-dependent heat production across the three genotypes. For all cases, differences were considered statistically significant at $P < 0.05$.

Data Availability. All study data are included in the article and/or supporting information.

ACKNOWLEDGMENTS. We thank Philip Hopkins and Paul Allen (University of Leeds) for providing the *RYR1* KI mice. ERTY was a generous gift from Young Tae Chang (National University of Singapore). We also thank D. George Stephenson (La Trobe University, Melbourne), James Hudson (Queensland Institute of Medical Research), and Razvan Cornea (University of Minnesota) for helpful comments on the manuscript. This work was supported by Australian Research Council Discovery Projects DP180100937 and DP200100435 (to B.S.L.).

1. J. Nowack, S. Giroud, W. Arnold, T. Ruf, Muscle non-shivering thermogenesis and its role in the evolution of endothermy. *Front. Physiol.* **8**, 889 (2017).
2. M. Periasamy, J. L. Herrera, F. C. G. Reis, Skeletal muscle thermogenesis and its role in whole body energy metabolism. *Diabetes Metab. J.* **41**, 327–336 (2017).
3. D. Scales, Giuseppeinesi, Assembly of ATPase protein in sarcoplasmic reticulum membranes. *Biophys. J.* **16**, 735–751 (1976).
4. I. C. Smith, E. Bombardier, C. Vigna, A. R. Tupling, ATP consumption by sarcoplasmic reticulum Ca^{2+} pumps accounts for 40-50% of resting metabolic rate in mouse fast and slow twitch skeletal muscle. *PLoS One* **8**, 1–11 (2013).
5. N. C. Bal *et al.*, Sarcolipin is a newly identified regulator of muscle-based thermogenesis in mammals. *Nat. Med.* **18**, 1575–1579 (2012).
6. N. C. Bal, S. K. Maurya, S. Singh, X. H. T. Wehrens, M. Periasamy, Increased reliance on muscle-based thermogenesis upon acute minimization of brown adipose tissue function. *J. Biol. Chem.* **291**, 17247–17257 (2016).
7. W. S. Smith, R. Broadbridge, J. M. East, A. G. Lee, Sarcolipin uncouples hydrolysis of ATP from accumulation of Ca2+ by the Ca2+-ATPase of skeletal-muscle sarcoplasmic reticulum. *Biochem. J.* **361**, 277–286 (2002).
8. G. J. Babu *et al.*, Ablation of sarcolipin enhances sarcoplasmic reticulum calcium transport and atrial contractility. *Proc. Natl. Acad. Sci. U.S.A.* **104**, 17867–17872 (2007).
9. A. Laganowsky *et al.*, Membrane proteins bind lipids selectively to modulate their structure and function. *Nature* **510**, 172–175 (2014).
10. A. R. P. Verkerke *et al.*, Phospholipid methylation regulates muscle metabolic rate through Ca^{2+} transport efficiency. *Nat. Metab.* **1**, 876–885 (2019).
11. H. Li, C. Wang, L. Li, L. Li, Skeletal muscle non-shivering thermogenesis as an attractive strategy to combat obesity. *Life Sci.* **269**, 119024 (2021).
12. J. M. Eltit *et al.*, RyR1-mediated Ca2+ leak and Ca2+ entry determine resting intracellular Ca2+ in skeletal myotubes. *J. Biol. Chem.* **285**, 13781–13787 (2010).
13. T. R. Cully *et al.*, Junctional membrane Ca^{2+} dynamics in human muscle fibers are altered by malignant hyperthermia causative RyR mutation. *Proc. Natl. Acad. Sci. U.S.A.* **115**, 8215–8220 (2018).
14. J. Aydin *et al.*, Nonshivering thermogenesis protects against defective calcium handling in muscle. *FASEB J.* **22**, 3919–3924 (2008).
15. B. A. Block, Thermogenesis in muscle. *Annu. Rev. Physiol.* **56**, 535–577 (1994).
16. B. A. Block, C. Franzini-Armstrong, The structure of the membrane systems in a novel muscle cell modified for heat production. *J. Cell Biol.* **107**, 1099–1112 (1988).
17. J. M. Morrissette, J. P. G. Franck, B. A. Block, Characterization of ryanodine receptor and Ca2+-ATPase isoforms in the thermogenic heater organ of blue marlin (*Makaira nigricans*). *J. Exp. Biol.* **206**, 805–812 (2003).
18. D. Bloemberg, J. Quadrilatero, Rapid determination of myosin heavy chain expression in rat, mouse, and human skeletal muscle using multicolor immunofluorescence analysis. *PLoS One* **7**, e35273 (2012).
19. V. Augusto, C. R. Padovani, G. E. R. Campos, Skeletal muscle fiber types in C57BL6J mice. *Braz. J. Morphol. Sci.* **21**, 89–94 (2004).
20. H. Brummer, M. Y. Zhang, M. Piddoubny, S. Medler, Hybrid fibers transform into distinct fiber types in maturing mouse muscles. *Cells Tissues Organs* **198**, 227–236 (2013).
21. T. Jordan, H. Jiang, H. Li, J. X. DiMario, Inhibition of ryanodine receptor 1 in fast skeletal muscle fibers induces a fast-to-slow muscle fiber type transition. *J. Cell Sci.* **117**, 6175–6183 (2004).
22. N. L. Thomas, A. J. Williams, Pharmacology of ryanodine receptors and Ca2+-induced Ca2+ release. *Wiley Interdiscip. Rev. Membr. Transp. Signal.* **1**, 383–397 (2012).
23. T. R. Cully, J. N. Edwards, R. M. Murphy, B. S. Launikonis, A quantitative description of tubular system Ca(2+) handling in fast- and slow-twitch muscle fibres. *J. Physiol.* **594**, 2795–2810 (2016).
24. X. Koenig, R. H. Choi, B. S. Launikonis, Store-operated Ca^{2+} entry is activated by every action potential in skeletal muscle. *Commun. Biol.* **1**, 31 (2018).
25. J. Paavola *et al.*, Mutant ryanodine receptors in catecholaminergic polymorphic ventricular tachycardia generate delayed afterdepolarizations due to increased propensity to Ca2+ waves. *Eur. Heart J.* **28**, 1135–1142 (2007).
26. D. Yang *et al.*, Ca2+/calmodulin kinase II-dependent phosphorylation of ryanodine receptors suppresses Ca2+ sparks and Ca2+ waves in cardiac myocytes. *Circ. Res.* **100**, 399–407 (2007).
27. T. R. Cully, J. N. Edwards, B. S. Launikonis, Activation and propagation of Ca2+ release from inside the sarcoplasmic reticulum network of mammalian skeletal muscle. *J. Physiol.* **592**, 3727–3746 (2014).
28. F. Dabertrand, M. T. Nelson, J. E. Brayden, Ryanodine receptors, calcium signaling, and regulation of vascular tone in the cerebral parenchymal microcirculation. *Microcirculation* **20**, 307–316 (2013).
29. S. Arai, S. C. Lee, D. Zhai, M. Suzuki, Y. T. Chang, A molecular fluorescent probe for targeted visualization of temperature at the endoplasmic reticulum. *Sci. Rep.* **4**, 6701 (2014).
30. H. Itoh *et al.*, Direct organelle thermometry with fluorescence lifetime imaging microscopy in single myotubes. *Chem. Commun. (Camb.)* **52**, 4458–4461 (2016).
31. C. R. Lamboley *et al.*, Ryanodine receptor leak triggers fibre Ca2+ redistribution to preserve force and elevate basal metabolism in skeletal muscle. *Sci. Adv.* **7**, eabi7144 (2021).
32. D. G. Stephenson, D. A. Williams, Calcium-activated force responses in fast- and slow-twitch skinned muscle fibres of the rat at different temperatures. *J. Physiol.* **317**, 281–302 (1981).
33. C. J. Barclay, B. S. Launikonis, Components of activation heat in skeletal muscle. *J. Muscle Res. Cell Motil.* **42**, 1–16 (2021).
34. M. G. Klein, L. Kovacs, B. J. Simon, M. F. Schneider, Decline of myoplasmic Ca2+, recovery of calcium release and sarcoplasmic Ca2+ pump properties in frog skeletal muscle. *J. Physiol.* **441**, 639–671 (1991).
35. M. W. Fryer, D. G. Stephenson, Total and sarcoplasmic reticulum calcium contents of skinned fibres from rat skeletal muscle. *J. Physiol.* **493**, 357–370 (1996).
36. L. de Meis, Uncoupled ATPase activity and heat production by the sarcoplasmic reticulum Ca2+-ATPase. Regulation by ADP. *J. Biol. Chem.* **276**, 25078–25087 (2001).
37. W. A. Macdonald, D. G. Stephenson, Effects of ADP on sarcoplasmic reticulum function in mechanically skinned skeletal muscle fibres of the rat. *J. Physiol.* **532**, 499–508 (2001).
38. V. A. Fajardo *et al.*, Co-expression of SERCA isoforms, phospholamban and sarcolipin in human skeletal muscle fibers. *PLoS One* **8**, e84304 (2013).
39. N. C. Bal *et al.*, Is upregulation of sarcolipin beneficial or detrimental to muscle function? *Front. Physiol.* **12**, 633058 (2021).
40. S. M. Gehrig *et al.*, Hsp72 preserves muscle function and slows progression of severe muscular dystrophy. *Nature* **484**, 394–398 (2012).
41. B. S. Launikonis *et al.*, Confocal imaging of [Ca2+] in cellular organelles by SEER, shifted excitation and emission ratioing of fluorescence. *J. Physiol.* **567**, 523–543 (2005).
42. X. Koenig *et al.*, Mechanistic insights into store-operated Ca^{2+} entry during excitation-contraction coupling in skeletal muscle. *Biochim. Biophys. Acta Mol. Cell Res.* **1866**, 1239–1248 (2019).
43. C. Franzini-Armstrong, Correction: The relationship between form and function throughout the history of excitation-contraction coupling. *J. Gen. Physiol.* **150**, 369 (2018).
44. G. D. Lamb, P. R. Junankar, D. G. Stephenson, Raised intracellular [Ca2+] abolishes excitation-contraction coupling in skeletal muscle fibres of rat and toad. *J. Physiol.* **489**, 349–362 (1995).
45. J. N. Edwards, B. S. Launikonis, The accessibility and interconnectivity of the tubular system network in toad skeletal muscle. *J. Physiol.* **586**, 5077–5089 (2008).
46. M. B. Cannell, D. G. Allen, Model of calcium movements during activation in the sarcomere of frog skeletal muscle. *Biophys. J.* **45**, 913–925 (1984).
47. C. J. Barclay, Energetics of contraction. *Compr. Physiol.* **5**, 961–995 (2015).